

Dynamic analysis of threshold characteristics and seasonal impact in the seasonal influenza SVEIRL model

*Ting Wang, Yunhu Zhang**

Lanzhou University of Technology, Lanzhou, China

*Corresponding Author. Email: zhangyh-17@163.com

Abstract. In this paper, a periodic seasonal influenza SVEIRL model is constructed to explore the mechanism by which seasonal influenza factors exert social impacts. Through dynamic analysis of the model and verification via numerical simulations, it is revealed that seasonal factors exhibit a significant positive correlation with both the basic reproduction number and the final epidemic scale. Using surveillance data from institutions including the Chinese National Influenza Center and the Public Health Science, the model is applied to simulate the trends of influenza epidemic in China. Under multi-dimensional scenarios that include different years, provinces, influenza subtypes, and the proportion of influenza-like cases in northern and southern regions of China, approximate values of seasonal factors for each scenario are calculated using methods such as genetic algorithms and parameter fitting. The findings reaffirm that the intensity of seasonal factors is positively correlated with the scale of influenza epidemics.

Keywords: seasonal influenza SVEIRL model, periodicity, threshold dynamics, final epidemic size

1. Introduction

Influenza has a significant threat to public health worldwide, whether in the form of pandemic, zoonotic, or seasonal influenza. Seasonal influenza (flu) is an acute respiratory infection caused by the influenza virus and is a common illness worldwide. Although most people recover without treatment, it still poses a considerable health burden. In temperate regions, seasonal influenza appears mainly in winter, while in tropical areas, it can occur throughout the year, causing more irregular outbreaks. There are approximately 1 billion cases of seasonal influenza each year, including 3 to 5 million severe cases [1-3]. Seasonal influenza leads to 290,000 to 650,000 respiratory deaths annually. It is noteworthy that 99% of flu-related respiratory infection deaths in children under 5 years old occur in developing countries. Symptoms generally start 1-4 days after infection and usually last about a week [4-6].

The influenza virus is divided into four types: A, B, C, and D. Types A and B are the main culprits behind seasonal influenza outbreaks. Seasonal influenza spreads quickly and easily in crowded places such as schools and nursing homes [3, 4]. When an infected person coughs or sneezes, droplets containing the virus are released into the air, which can infect people in the vicinity. The virus can also be transmitted through contact with hands that are contaminated with the influenza virus [7-10].

A multitude of studies have shown that the incidence of seasonal influenza varies significantly among different populations [2, 3, 11-13]. For example, in 2014, Xiaofei Fu et al. analyzed the role of different age groups in influenza epidemics using the moving average method to identify the epidemic waves of influenza-like cases. They concluded that younger age groups were the first to become ill during seasonal influenza outbreaks and suggested prioritizing the affected population when new strains of influenza emerge [2]. There are also differences in seasonal influenza by gender. In 2020, Quanfu Zhang et al. used the immunogold method to perform rapid antigen detection of influenza A and B viruses in nasopharyngeal swab specimens from influenza-like cases. They found that the proportion of men infected with influenza A was significantly higher than that of women, while the proportion of women infected with influenza B was notably higher than that of men [12]. In addition, in 2016, Clara Stegehuis and Remco van der Hofstad explored the impact of community structure on the spread of epidemics through the analysis of real network data-sets from six different fields. Their study revealed that high-density connections between communities are the main reason for the spread of diseases [11]. In 2021, Miled EI Hajji et al. Researched an SVEIR infectious disease model that considers seasonal environmental impacts, exploring the dynamics of disease transmission and corresponding control strategies through mathematical analysis [3]. In 2022, Enrique C. Gabrick et al. studied the impact of vaccination on disease transmission in seasonal infectious disease models. By introducing regular vaccination strategies for newborns and susceptible populations, they analyzed the impact of vaccination strategies on infection peaks and the cumulative number of infected individuals, establishing a SEIRS seasonal model [13].

However, many communicable diseases exhibit widespread periodic characteristics, which can be influenced by seasonal fluctuations in contact rates. These fluctuations are primarily attributed to social and individual behaviors, such as temporal patterns in different regions and individual incidence time series, as well as changes in climatic conditions. To address this, this study examines the potential seasonal patterns of influenza incidence, incorporating environmental factors such as sunlight intensity and temperature, and establishes a seasonal influenza SVEIRL model.

The structure of this paper is as follows: In Section 2, the SVEIRL model with seasonal fluctuations of period T is proposed. In Section 3, the dynamics of the SVEIRL model are analyzed, and the threshold characteristics are discussed. Through calculations, we are shown that there is a positive correlation between seasonal factors and both the basic reproduction number and the final epidemic size. In Section 4, numerical simulations are conducted by adjusting the model parameters to further verify their relationships. Finally, in Section 5, a brief conclusion is presented.

2. SVEIRL model with seasonal cycles of period

The seasonal cycle of the influenza virus is formed by the combined action of multiple factors [5]. Among these, the cold winters in high-latitude regions, large-scale population movements driven by human activities, and weather events are all important factors affecting the spread of the influenza virus. In addition, the influenza virus has the ability to mutate rapidly, introducing new strains to evade the protection of the human immune system. This results in a rapid replenishment of the number of susceptible individuals and a shortened expected duration of the epidemic [14, 15]. Therefore, the seasonal cycle of the influenza virus is the result of the interaction of various factors such as climate and human behavior. For example, in 2022, Nico Stollenwerk et al. proposed a seasonal SIRS compartment model with periodic driving $S(t) = 1 + a\cos(\omega t)$ [16]. In 2023, Joel Wagner, Simon Bauer, and Sebastian Contrera also studied a seasonal respiratory disease model with rapidly mutating pathogens and provided seasonal forcing for the infection rate $\beta(t) = \beta_0[1 + \sigma\cos\omega(t + \varphi)]$.

They proposed a corresponding model with periodic vaccination, incorporating seasonality into the model [17]. To this end, considering the influence of seasonal forcing on the spread of the epidemic, we present a sea-sonal fluctuation equation with a period of T in the section, where the parameter $\beta_1 = a_1 + b_1 \sin(\omega t)$ and $\beta_2 = a_2(1 + b_2 \sin(\omega t))$ represent the transmission rates of periodic seasonal fluctuations. Additionally, we put the model take into account various multi-layered related factors of seasonality, including environmental factors such as sunlight intensity and temperature, as well as vaccination, individual immunity and population mobility. Finally, we will divide the population into susceptible subgroups $S(t)$,vaccinate subgroups $V(t)$, exposed subgroups $E(t)$, symptom subgroups $I(t)$, virus carrying subgroups $L(t)$, and recovery subgroup $R(t)$. The total population is denoted as $N(t) = S(t) + V(t) + E(t) + I(t) + L(t) + R(t)$, and an SVEIRL model with six subgroups is established. We are assumed that the number of births per month is constant. After being infected, susceptible individuals first enter the latent period. During this period, they will not show symptoms and will not infect others. Approximately 1 to 4 days later, these individuals will become infectious. The model structure diagram is shown below (Figure 1).

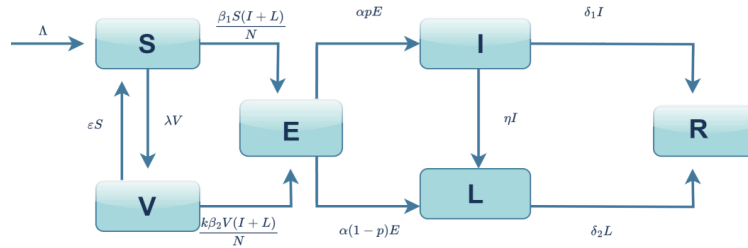


Figure 1. The flow chart of SVEILR model

$$\begin{aligned}
 \frac{dS}{dt} &= \Lambda + \lambda V - \left[\frac{\beta_1(t)(I+L)}{N} + \epsilon + \mu \right] S, \\
 \frac{dV}{dt} &= \epsilon S - \left[\frac{k\beta_2(t)(I+L)}{N} + \lambda + \mu \right] V, \\
 \frac{dE}{dt} &= \beta_1(t)S\left(\frac{I+L}{N}\right) + k\beta_2(t)V\left(\frac{I+L}{N}\right) - (\alpha + \mu)E, \\
 \frac{dI}{dt} &= \alpha\rho E - (\eta + \delta_1 + \mu)I, \\
 \frac{dL}{dt} &= \alpha(1 - \rho)E + \eta I - (\delta_2 + \mu)L, \\
 \frac{dR}{dt} &= \delta_1 I + \delta_2 L - \mu R.
 \end{aligned} \tag{1}$$

Since the last equation can be decoupled from the see Equations (1), the system the system becomes see Equations (2):

$$\begin{aligned}
 \frac{dS}{dt} &= \Lambda + \lambda V - \left[\frac{\beta_1(t)(I+L)}{N} + \epsilon + \mu \right] S, \\
 \frac{dV}{dt} &= \epsilon S - \left[\frac{k\beta_2(t)(I+L)}{N} + \lambda + \mu \right] V, \\
 \frac{dE}{dt} &= \beta_1(t)S\left(\frac{I+L}{N}\right) + k\beta_2(t)V\left(\frac{I+L}{N}\right) - (\alpha + \mu)E, \\
 \frac{dI}{dt} &= \alpha\rho E - (\eta + \delta_1 + \mu)I, \\
 \frac{dL}{dt} &= \alpha(1 - \rho)E + \eta I - (\delta_2 + \mu)L.
 \end{aligned} \tag{2}$$

For convenience in calculation and representation, let $\varphi_4 = \eta + \delta_1 + \mu$, $\varphi_5 = \delta_2 + \mu$, $\varphi_1 = \epsilon + \mu$, $\varphi_2 = \lambda + \mu$, $\varphi_3 = \alpha + \mu$, then the model (see Equations (1)) becomes the following form

(Equations (3)).

$$\begin{aligned}\frac{dS}{dt} &= \Lambda + \lambda V - \left[\frac{\beta_1(t)(I+L)}{N} + \varphi_1 \right] S, \\ \frac{dV}{dt} &= \varepsilon S - \left[\frac{k\beta_2(t)(I+L)}{N} + \varphi_2 \right] V, \\ \frac{dE}{dt} &= \beta_1(t)S\left(\frac{I+L}{N}\right) + k\beta_2(t)V\left(\frac{I+L}{N}\right) - \varphi_3 E, \\ \frac{dI}{dt} &= \alpha \rho E - \varphi_4 I, \\ \frac{dL}{dt} &= \alpha(1 - \rho)E + \eta I - \varphi_5 L.\end{aligned}\tag{3}$$

add the above five equations together, we get Equation (4):

$$\frac{dN}{dt} = \Lambda - \mu N.\tag{4}$$

Where the initial value is Equation (5):

$$S(0) = S_0, V(0) = V_0, E(0) = E_0, I(0) = I_0, R(0) = R_0.\tag{5}$$

and there is a feasible area (Equation (6)):

$$D = \{(S, V, E, I, L, R) | S + V + E + I + L + R \leq \frac{\Lambda}{\mu}\}.\tag{6}$$

To begin with, the model diagram is depicted in see Figure 1. Here, δ_1 and δ_2 can incorporate factors such as individual immunity, natural immunity or social influence, and medical resources.

3. Dynamic analysis of the SVEIRL model

To facilitate the discussion on the dynamic threshold of the model (3), we first discuss the positivity and boundedness of the model (3) (see Equations (1)).

Theorem 1. *If the initial value $\{S(0), V(0), E(0), I(0), L(0), R(0)\}$ is positive, then the solution of the model (3) (see Equations (1)) $\{S(t), V(t), E(t), I(t), L(t), R(t)\}$ is persistence and bounded for all $t \in [0, +\infty)$.*

Proof In model (3) (see Equations (1)), given that the solution corresponding to the initial value is continuous, it is sufficient to demonstrate that the solution set $\{S(t), V(t), E(t), I(t), L(t), R(t)\}$ remains positive for all $t \in [0, +\infty)$, provided that the initial values $\{S(0), V(0), E(0), I(0), L(0), R(0)\}$ are positive. Commencing from the first equation of the model, we observe Equation (7):

$$\frac{dS}{dt} = [\beta_S(t)\frac{I+L}{N} + \varepsilon + \mu]S(t).\tag{7}$$

Consequently, given that $S(0) > 0$, we directly have $S(t) > 0$ for all $t \in [0, +\infty)$.

Subsequently, which define $Y(t) = \min\{S(t), V(t), E(t), I(t), L(t), R(t)\}$, clearly $Y(0) = \min\{S(0), V(0), E(0), I(0), L(0), R(0)\} > 0$. To establish this theorem, we are sufficient to demonstrate that $Y(t) > 0$ for all $t \in [0, t_0)$. Suppose there exists a time point t such that $t \in [0, t_0)$ and $Y(t_0) = 0$, then consider the following five scenarios (Equations (8)):

$$\begin{aligned}Y(t_0) &= E(t_0); \\ Y(t_0) &= V(t_0); \\ Y(t_0) &= I(t_0); \\ Y(t_0) &= L(t_0); \\ Y(t_0) &= R(t_0);\end{aligned}\tag{8}$$

It is rational to assume that $Y(0) = V(0)$, at that time $t \in [0, t_0]$. From the second equation of the model (3) (see Equations (1)), the study derives the following inequality (Equation (9)):

$$\frac{dV}{dt} \geq (k\beta_2(t)\frac{I+L}{N} + \mu)V(t). \tag{9}$$

this inequality holds for all $t \in [0, t_0]$. By invoking the comparison principle, we obtain Equation (10):

$$V(t_0) > V(0)e^{-(k\beta_2(t)\frac{I+L}{N} + \mu)t} > 0. \tag{10}$$

This result contradicts the assumption that $V(t_0) > 0$. By analogous reasoning, we can demonstrate that other scenarios also lead to contradictions. Consequently, the solution of the model (3) (see Equations (1)) remains positive for all $t \in [0, t_0]$.

Given that $N = S + V + E + I + L + R$, we have Equation (11):

$$\frac{dN}{dt} = \frac{dS}{dt} + \frac{dV}{dt} + \frac{dE}{dt} + \frac{dI}{dt} + \frac{dL}{dt}. \tag{11}$$

Substituting the model (3) (see Equations (1)) equations and rearranging them yields

$$\frac{dN}{dt} = \Lambda - \mu N. \tag{12}$$

Since $\Lambda \geq 0$, it follows that $\frac{dN}{dt} \leq \Lambda - \mu N$. Consequently, the model (3) (see Equations (1)) possesses a positive invariant region

$$D = \{(S, V, E, I, L, R) | S + V + E + I + L + R \leq \frac{\Lambda}{\mu}\}. \tag{13}$$

All solutions of the model are confined within this positive invariant region, which ensures the boundedness of the model (3) (see Equations (1)).

The basic reproduction number R_0 of model (3) (see Equations (1)) is defined below. The basic reproduction number R_0 is, in essence, the spectral radius of the next generation matrix. This concept was initially put forward by Diekmann et al. In 1990 and 2002, Van den Driessche and Watmough introduced a relatively simpler method for its calculation. As a critical threshold in epidemic models, R_0 indicates the average number of people an infected individual can infect during their average infectious period when the entire population is susceptible. It determines whether an epidemic R_0 will occur [18]. The methods for calculating the basic reproduction number include the next generation matrix method and the maximum likelihood function method. Here, the next generation matrix method is applied to calculate.

Theorem 2. *For model (3) (see Equations (1)), the study indicates that the disease will not outbreak on a large scale when $R_0 \leq 1$. Conversely, when $R_0 > 1$, the disease will outbreak; whereas when $R_0 < 1$, the disease will tend to disappear.*

Proof To derive the basic reproduction number R_0 , the isolated basic reproduction number for a single population i is calculated. Consequently, we initially focus on model (3) (see Equations (1)). It is essential to differentiate between the newly infected population and other population changes. Therefore, the newly infected and transition terms of model (3) (see Equations (1)) are defined separately $F(t)$ and $V(t)$. The Jacobian matrices of the infection components S, V, E, I and L at the disease-free equilibrium point

$$P_0 = (S_0, V_0, 0, 0, 0) = (\frac{\Lambda}{\varphi_1 - \lambda V}, \frac{\varepsilon S}{\varphi_2}, 0, 0, 0) \tag{14}$$

are as follows Equations (15):

$$J_F(P_0) = \begin{bmatrix} \beta_1(t)\frac{I+L}{N} + k\beta_2(t)\frac{I+L}{N} & \alpha\rho & \alpha(1-\rho) \\ 0 & 0 & 0 \\ 0 & 0 & 0 \end{bmatrix}, \tag{15}$$

$$J_V(P_0) = \begin{vmatrix} \varphi_3 & 0 & 0 \\ 0 & \varphi_4 & 0 \\ 0 & 0 & \varphi_5 \end{vmatrix}. \tag{16}$$

then

$$J_F^{-1} J_V = \begin{bmatrix} (\beta_1(t) \frac{I+L}{N} + k\beta_2(t) (\frac{I+L}{N}) \varphi_3^{-1}) & \frac{\alpha\rho}{\varphi_4} & \frac{\alpha(1-\rho)}{\varphi_5} \\ 0 & 0 & 0 \\ 0 & 0 & 0 \end{bmatrix}. \tag{17}$$

therefore, the basic reproduction number of model (3) (see Equations (1)) is

$$R_0 = \rho(J_F J_V^{-1}) = \frac{\beta_1(t)(I+L) + k\beta_2(t)(I+L)}{\varphi_3 N} + \frac{\alpha\rho}{\varphi_4} + \frac{\alpha}{(1-\rho)} \varphi_5. \tag{18}$$

Through the calculation of (16), it can be concluded that when $R_0 = 1$, it is equivalent to

$$(\beta_1(t) + k\beta_2(t))(I + L) = \varphi_3 N [1 - (\frac{\alpha\rho}{\varphi_4} + \frac{\alpha(1-\rho)}{\varphi_5})]. \tag{19}$$

This indicates that the disease will not outbreak on a large scale when $R_0 \leq 1$. Conversely, when $R_0 > 1$, the disease will outbreak; whereas when $R_0 < 1$, the disease will tend to disappear.

Below we discuss the stability at the disease-free equilibrium point $(S_0, V_0, 0, 0, 0) = (\frac{\Lambda}{\varphi_1 - \lambda V}, \frac{\varepsilon S}{\varphi_2}, 0, 0, 0)$ in model (3).

Theorem 3. When $R_0 < 1$, the disease-free equilibrium point $(S_0, V_0, 0, 0, 0) = (\frac{\Lambda}{\varphi_1 - \lambda V}, \frac{\varepsilon S}{\varphi_2}, 0, 0, 0)$, is locally asymptotically stable; when $R_0 > 1$, it is unstable.

Proof The Jacobian matrix of the model (3) (see Equations (1)) at the disease-free equilibrium point $P_0 = (S_0, V_0, 0, 0, 0) = (\frac{\Lambda}{\varphi_1 - \lambda V}, \frac{\varepsilon S}{\varphi_2}, 0, 0, 0)$ can be expressed as see Equations (18).

$$J(P_0) = \begin{bmatrix} -\varphi_1 & \lambda & 0 & -\frac{\beta_1(t)S_0}{N} & -\frac{\beta_1(t)S_0}{N} \\ \varepsilon & -\varphi_2 & 0 & -\frac{k\beta_2(t)V_0}{N} & -\frac{k\beta_2(t)V_0}{N} \\ 0 & 0 & -\varphi_3 & \frac{\beta_1(t)S_0 + k\beta_2(t)V_0}{N} & \frac{\beta_1(t)S_0 + k\beta_2(t)V_0}{N} \\ 0 & 0 & \alpha\rho & -\varphi_4 & 0 \\ 0 & 0 & \alpha(1-\rho) & \eta & -\varphi_5 \end{bmatrix}. \tag{20}$$

Among which $S_0 = \frac{\Lambda}{\varphi_1 - \lambda V}$, $V_0 = \frac{\varepsilon S}{\varphi_2}$. The essay can simplify (18) to obtain $(-\varphi_3 - \lambda)(-\varphi_4 - \lambda)(-\varphi_5 - \lambda)[(-\varphi_1 - \lambda)(-\varphi_2 - \lambda) - \lambda\varepsilon] = 0$.

Therefore, we have the eigenvalues (18) as

$$\lambda_1 = -\varphi_3, \lambda_2 = -\varphi_4, \lambda_3 = -\varphi_5, \lambda_4 = \frac{-(\varphi_1 + \varphi_2 - \varepsilon) + \sqrt{(\varphi_1 + \varphi_2 - \varepsilon)^2 - 4\varphi_1\varphi_2}}{2}, \lambda_5 = \frac{-(\varphi_1 + \varphi_2 - \varepsilon) - \sqrt{(\varphi_1 + \varphi_2 - \varepsilon)^2 - 4\varphi_1\varphi_2}}{2}$$

Next, we will only discuss the cases where the real parts of λ_4 and λ_5 are negative. Let $\Delta = (\varphi_1 + \varphi_2 - \varepsilon)^2 - 4\varphi_1\varphi_2$, which discuss the cases as follows:

- When $\Delta \geq 0$: λ_4 and λ_5 are real numbers. To make $\lambda_4 < 0$ and $\lambda_5 < 0$, first, the numerator $-(\varphi_1 + \varphi_2 - \varepsilon) \pm \sqrt{(\varphi_1 + \varphi_2 - \varepsilon)^2 - 4\varphi_1\varphi_2} < 0$.

Since $\sqrt{(\varphi_1 + \varphi_2 - \varepsilon)^2 - 4\varphi_1\varphi_2} \geq 0$, we only need $-(\varphi_1 + \varphi_2 - \varepsilon) < 0$, that is, $\varphi_1 + \varphi_2 - \varepsilon > 0$.

- When $\Delta < 0$: λ_4 and λ_5 are conjugate complex numbers. The real parts are both $Re(\lambda_4) = Re(\lambda_5) = \frac{-(\varphi_1 + \varphi_2 - \varepsilon)}{2}$. To make the real parts negative, which also need to satisfy $\varphi_1 + \varphi_2 - \varepsilon > 0$.

Therefore, according to seeing Equations (16), if the above-mentioned conditions are reasonable, which are equivalent to $R_0 < 1$, and all the eigenvalues of the model have negative real parts. Thus, we have just completed the proof of this theorem.

Theorem 4. When $R_0 < 1$, the disease-free equilibrium point $(S_0, V_0, 0, 0, 0) = (\frac{\Lambda}{\varphi_1 - \lambda V}, \frac{\epsilon S}{\varphi_2}, 0, 0, 0)$ is globally asymptotically stable.

Proof Construct the Lyapunov function

$$V(S, V, E, I, L, R) = S - S_0 - S_0 \ln(\frac{S}{S_0}) + V - V_0 - V_0 \ln(\frac{V}{V_0}) + E + I + L + R.$$

According to the chain rule

$$\frac{dV}{dt} = \frac{\partial V}{\partial S} \frac{dS}{dt} + \frac{\partial V}{\partial V} \frac{dV}{dt} + \frac{\partial V}{\partial E} \frac{dE}{dt} + \frac{\partial V}{\partial I} \frac{dI}{dt} + \frac{\partial V}{\partial L} \frac{dL}{dt} + \frac{\partial V}{\partial R} \frac{dR}{dt}. \tag{21}$$

First, the study calculates the partial derivatives

$$\frac{\partial V}{\partial S} = 1 - \frac{S_0}{S}, \frac{\partial V}{\partial V} = 1 - \frac{V_0}{V}, \frac{\partial V}{\partial E} = 1, \frac{\partial V}{\partial I} = 1, \frac{\partial V}{\partial L} = 1, \frac{\partial V}{\partial R} = 1. \tag{22}$$

Substitute the partial derivatives and the differential equation into the expression of $\frac{dV}{dt}$.

$$\frac{\partial V}{\partial S} \frac{dS}{dt} = (1 - \frac{S_0}{S})[\Lambda + \lambda V - (\frac{\beta_1(t)(I+L)}{N} + \varphi_1)S] = \Lambda - \frac{\Lambda S_0}{S} + \lambda V - \frac{\lambda V S_0}{S} - (\frac{\beta_1(t)(I+L)}{N} + \varphi_1)S + (\frac{\beta_1(t)(I+L)}{N} + \varphi_1)S_0.$$

$$\frac{\partial V}{\partial V} \frac{dV}{dt} = (1 - \frac{V_0}{V})[\epsilon S - (\frac{k\beta_2(t)(I+L)}{N} + \varphi_2)V] = \epsilon S - \frac{\epsilon S V_0}{V} - (\frac{k\beta_2(t)(I+L)}{N} + \lambda + \mu)V + (\frac{k\beta_2(t)(I+L)}{N} + \varphi_2)V_0. \tag{23}$$

$$\frac{\partial V}{\partial E} \frac{dE}{dt} = \beta_1(t)S(\frac{I+L}{N}) + k\beta_2(t)V(\frac{I+L}{N}) - \varphi_3 E.$$

$$\frac{\partial V}{\partial I} \frac{dI}{dt} = \alpha \rho E - \varphi_4 I. \tag{24}$$

$$\frac{\partial V}{\partial L} \frac{dL}{dt} = \alpha(1 - \rho)E + \eta I - \varphi_5 L.$$

$$\frac{\partial V}{\partial R} \frac{dR}{dt} = \delta_1 I + \delta_2 L - \mu R.$$

Combine similar terms to obtain

$$\begin{aligned} \frac{dV}{dt} = & \Lambda - \frac{\Lambda S_0}{S} + \lambda V - \frac{\lambda V S_0}{S} - (\frac{\beta_1(t)(I+L)}{N} + \varphi_1)S + (\frac{\beta_1(t)(I+L)}{N} + \varphi_1)S_0 + \epsilon S - \frac{\epsilon S V_0}{V} - (\frac{k\beta_2(t)(I+L)}{N} \\ & + \varphi_2)V + (\frac{k\beta_2(t)(I+L)}{N} + \varphi_2)V_0 + \beta_1(t)S(\frac{I+L}{N}) + k\beta_2(t)V(\frac{I+L}{N}) - \varphi_3 E + \alpha \rho E - \varphi_4 I + \alpha(1 - \rho)E \\ & + \eta I - \varphi_5 L + \delta_1 I + \delta_2 L - \mu R. \end{aligned} \tag{25}$$

When $R_0 < 1$, based on the disease-free equilibrium $(S_0, V_0, 0, 0, 0)$, one can obtain that $\frac{dV}{dt} < 0$; and there exists a positive invariant set

$$D = \{(S, V, E, I, L, R) | S + V + E + I + L + R \leq \frac{\Lambda}{N}\}. \tag{26}$$

So, when $\frac{dV}{dt} = 0$, we found that except for the disease-free equilibrium point, the system cannot maintain $\frac{dV}{dt} = 0$ at other points. This is because V is positive definite, and $\frac{dV}{dt} = 0$. In addition to the disease-free equilibrium point, $\frac{dV}{dt}$ is not always 0. According to Lyapunov stability theory, the disease-free equilibrium point $(S_0, V_0, 0, 0, 0)$ of this infectious disease model is globally asymptotically stable.

Next, we divide $\frac{dS}{dt}$, $\frac{dV}{dt}$ in (3) (see Equations (1)) by S , V on both side, have (3) (see Equations (1))

$$\frac{dS}{S} = \frac{\Lambda}{S} + \frac{\lambda V}{S} - [\beta_I(t) \frac{I+L}{N}] - \varphi_1, \tag{27}$$

$$\frac{dV}{V} = \frac{\epsilon S}{V} - (\beta_V(t) \frac{I+L}{N}) - \varphi_2.$$

for see Equations (3), during the entire epidemic transmission period from \int_0^∞ for t on both sides obtain

$$\begin{aligned} \log \frac{S(\infty)}{S(0)} &= -\varphi_1 + \int_0^\infty (\frac{\Lambda}{S} + \frac{\lambda V}{S} - [\beta(t) \frac{I+L}{N}]) dt, \\ \log \frac{V(\infty)}{V(0)} &= -\varphi_2 + \int_0^\infty (\frac{\epsilon S}{V} - (k\beta(t) \frac{I+L}{N})) dt. \end{aligned} \tag{28}$$

There are numerous methods to define the final size of an epidemic [19]. For instance, in [20], the SIR model with demographic stochastic noise and its extended epidemiological models are employed to calculate the probability distribution of all widespread outbreaks under large population constraints. The final epidemic scale is defined by calculating the outbreak probability distribution. In [21], a random branching process is used to describe the onset of disease outbreaks. It is proposed that, unlike interval models, if the basic reproduction number is greater than 1, small-scale outbreaks or pandemics may occur. The likelihood of this depends on the nature of the contact network, and network methods are used to determine the distribution of outbreak and pandemic scales. In [22], by analyzing the distribution and scale of the floating population at the provincial level across the country and at the prefecture level in Hubei Province, and based on the characteristics of virus transmission, the scale estimates were grouped by age group, type of family migration, number of family migrants, household registration type, and reasons for migration. These were then summarized by administrative region. Additionally, factors such as the type of population controlling the spread of the virus, medical interventions, government control measures, and statistical reports were considered to estimate the development of the epidemic in various regions based on the scale of the floating population in Wuhan and the daily confirmed cases. From the perspective of population movement and the number of confirmed cases, the final epidemic scale is defined here by comparing the number of susceptible individuals and vaccinated individuals between the initial state and the final state. For example, we define a metric F that represents the final prevalence index.

Definition 1. *The final epidemic size of every single group i in system (3) (see Equations (1)) is*

$$F = \frac{(S(\infty) - S(0)) - (V(\infty) - V(0))}{S(0)}. \quad (29)$$

In the discussion of this section, based on see Equations (18) and (29) we can be concluded that the seasonal factors are positively correlated with the basic reproduction number and the final epidemic size. In the next section, through numerical simulations, the model parameters will be altered to further elucidate this relationship.

4. Numerical simulation

In this section, we further verify the relationship between seasonal factors and the basic reproduction number, as well as the final epidemic size about the model (3). The section we first simulate the relationship between the basic reproduction number R_0 affected by seasonal factors a_1, a_2, b_1, b_2 (see Figure 2), and the proportional relationship between them (see Figure 3) through adjusting the relevant parameters of the model (3). The results show that the seasonal factors are positively correlated with the basic reproduction number are positively correlated. Subsequently, we model the final size of the five different populations in relation to the total population over time (see Figure 4), and the relationship between the final epidemic scale F and seasonal factors a_1, a_2, b_1, b_2 is simulated (see Figure 5). The results show that when the number of susceptible individuals far exceeds the number of infected individuals, disease outbreaks continue for a period of time. When the number of infected individuals is almost equal to the number of cases, the disease will have small outbreaks for a period of time and eventually stabilize in the area. When the number of infected individuals is less than the number of cases, the disease eventually disappears after a period of time.

Finally, based on the data from the Chinese Influenza Center and the Public Health Science, we conduct simulations on the influenza situation in China and incorporate the data into the SVEIRL model. We then estimate the ranges of seasonal factors for influenza in China under different scenarios, including different years in China and seasonal factors impact (see Figure 6, see Figure 7, see Figure 8 and see Figure 9),

Different provinces in China and seasonal factors impact (see Figure 10 and see Figure 11), Flu scenarios kinds in China and seasonal factors impact (see Figure 12, see Figure 13, see Figure 14) and ILI (%) of South and north in China and seasonal factors impact (see Figure 15). By establishing the heritage algorithm and parameter fitting methods, nonlinear optimization and least square methods, combined with the model (3), we calculate the approximate values of the seasonal factors related. By establishing the heritage algorithm and parameter fitting methods, nonlinear optimization and least square methods, combined with the model (3), we calculate the approximate values of the seasonal factors related to the influenza epidemic in Chinese these different scenarios and once again confirm that there is a positive correlation between the seasonal factors and the scale of the influenza epidemic.

4.1. Reproduction number and seasonal factors impact

Here, we simulate the relationship of reproduction number R_0 and the impact of seasonal factors. The diagrams of the basic reproduction number R_0 affected by seasonal factors a_1, a_2, b_1, b_2 (see Figure 2), as well as the relationships between their ratios (see Figure 3) for model (3). We find that seasonal factors are positively correlated with the basic reproduction number, and the sine relationship graph of the basic reproduction number over time (see Figure 2). In the figure, labeled as Group1, Group2, Group3, Group4, and Group5, and represented by different colored lines.

We observe that as the seasonal factors increase, the basic number of births increases correspondingly, and the frequency of oscillation becomes more intense. In this section we find that as time increases, when the ratio of a_1/a_2 and b_1/b_2 increases, the basic reproduction number R_0 will increase; and the effect of the increase will be more pronounced see Figure 3.

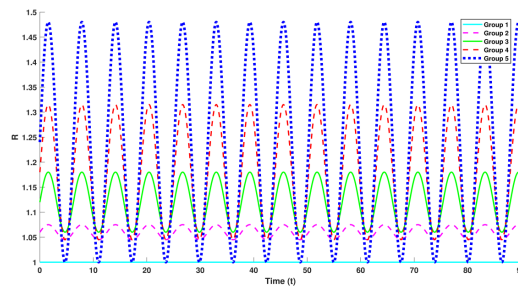


Figure 2. The sine relationship graph of the basic reproduction number R_0 over time is presented. Five sets of values for the seasonal factors are taken at equal intervals $(a_1, a_2, b_1, b_2) = (0, 0, 0, 0); (0.5, 0.25, 0.5, 0.25); (1, 0.5, 1, 0.5); (1.5, 0.75, 1.5, 0.75); (2, 1, 2, 1)$, namely. In the figure, these sets are labeled as Group1, Group2, Group3, Group4, and Group5, and represented by different colored lines. It is observed that as the seasonal factors increase, the basic reproduction number correspondingly increases, and the frequency of oscillation becomes more intense

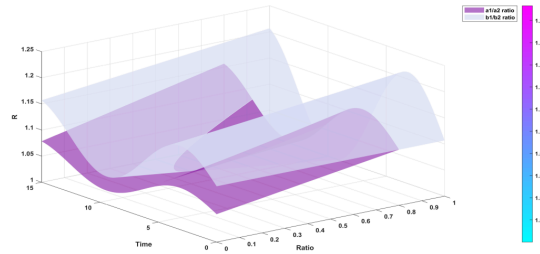


Figure 3. The graph depicts the relationship over time between the basic reproduction number R_0 and the ratio of the seasonal factors a_1, a_2 and $b_1 = 0.5, b_2 = 0.5$. Here, the study takes $I = L = 10^4, k = 0.8, N = 10^6$. For the ratio of the seasonal factors a_1, a_2 , we fix values $b_1 = 0.5, b_2 = 0.5$, while varying $\frac{a_1}{a_2}$ within the range $[0, 0.8]$; for the ratio of the seasonal factors b_1, b_2 , we fix values $a_1 = 1, a_2 = 1$, while varying b_1/b_2 within the range $[0, 1]$. It is found that as time $\frac{a_1}{a_2}$ and $\frac{b_1}{b_2}$ increases, the basic reproduction number rises when the ratio increases, with the effect becoming more pronounced as the ratio increases

4.2. Final scales of populations and seasonal factors impact

Here, we simulate the relationship final scales F of population and seasonal factors impact for model (3). We consider the introduction of trends see Figure 4(a): The relationship between the final scale of the growth of the flu outbreak in five different groups of people $F_i (i = 1, 2, 3, 4, 5)$ and the total population F over time is simulated. We then put the groups are represented by Group1, Group2, Group3, Group4, Group5, and Total, with different lines indicating different groups. The respective population sizes are as follows:

- Group1: $(S, V, I, L) = (10^4, 10^3, 10^3, 10^3)$;
- Group2: $(S, V, I, L) = (9 \times 10^3, 1.5 \times 10^3, 2 \times 10^3, 1.5 \times 10^3)$;
- Group3: $(S, V, I, L) = (8 \times 10^3, 2 \times 10^3, 3 \times 10^3, 2 \times 10^3)$;
- Group4: $(S, V, I, L) = (7 \times 10^3, 2.5 \times 10^3, 4 \times 10^3, 2.5 \times 10^3)$;
- Group5: $(S, V, I, L) = (6 \times 10^3, 3 \times 10^3, 5 \times 10^3, 3 \times 10^3)$.

The total population $N = 2 \times 10^4$. The parameters are $\phi_1 = \phi_2 = \Delta = \lambda = \epsilon = 0.5, a_1 = 0.5, a_2 = 0.6, b_1 = 0.8, b_2 = 0.7, k = 0.8$. Let the number of susceptible individuals gradually decrease, while the number of virus carriers, mild symptom individuals, and severe symptom individuals gradually increase. The graph shows that the final epidemic scale F of the disease is related to the number of susceptible individuals. When the number of susceptible individuals is at its highest, ignoring other factors, the final epidemic scale F of the disease will also increase. When the number of infected individuals far exceeds the number of sick individuals, the disease will continue to break out for a period of time. When the number of infections is almost equal to the number of cases, the disease will have small-scale outbreaks for a period of time, eventually leveling off in the region.

Increasing the data scale see Figure 4(b): simulate and hypothesize the relationship between the final size of five different groups of large-scale populations and the total population over time. The groups are represented by Group1, Group2, Group3, Group4, Group5, and Total, with different lines representing different groups. The respective population sizes are as follows:

- Group1: $(S, V, I, L) = (10^4, 8^4, 7^4, 5^4)$;
- Group2: $(S, V, I, L) = (9 \times 10^3, 5 \times 10^4, 6 \times 10^4, 4 \times 10^4)$;
- Group3: $(S, V, I, L) = (8 \times 10^4, 5 \times 10^4, 4 \times 10^4, 4 \times 10^4)$;
- Group4: $(S, V, I, L) = (4.5 \times 10^5, 4 \times 10^4, 6 \times 10^3, 2 \times 10^4)$;
- Group5: $(S, V, I, L) = (5 \times 10^5, 5 \times 10^4, 8 \times 10^4, 7 \times 10^4)$.

the total population $N = 10^7$. The parameters are $\phi_1 = \phi_2 = \Delta = \lambda = \epsilon = 0.5, a_1 = 0.5, a_2 = 0.6, b_1 = 0.8, b_2 = 0.7, k = 0.8$.

Therefore, we illustrate that when the number of susceptible individuals significantly exceeds the number of infected individuals, the disease continues to spread over a period of time. When the number of infected individuals is nearly equal to the number of sick individuals, the disease experiences small-scale outbreaks for a period before eventually stabilizing in the region. Conversely, when the number of infected individuals is less than the number of sick individuals, the disease will eventually fade out after a period of time (see Figure 4).

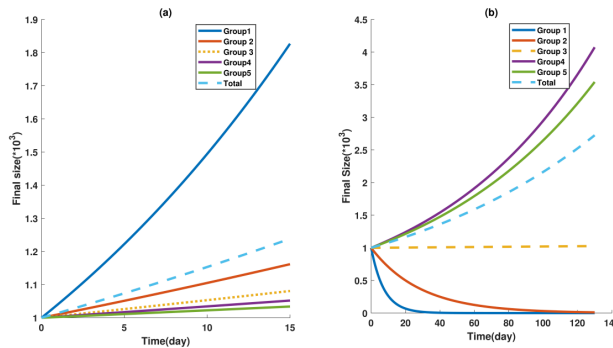


Figure 4. The relationship graph depicts the final scale F of five different groups and the total population F over time. (a). Considering the introduction of trends, the study simulates the relationship between the final scale of five different groups and the total population during influenza outbreak growth over time. (b). Considering an increase in the data scale, the study simulates hypothetical studies on the final scale of five different groups and the total population in large-scale populations over time

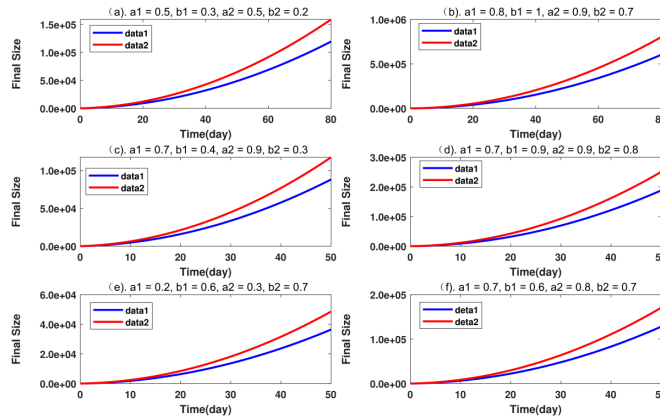


Figure 5. The graph illustrates the relationship between the final epidemic scale F and time under different seasonal factor variations. Here, the study focus on two populations, Group 1 and Group 2, represented by blue and red curves, respectively. The study examines three scenarios: (a, b): Seasonal factors are different. In the left graph, their values are set between 0 and 0.5, while in the right graph, their values are increased to 0.5 and 1. (c, d): With the values of a_1 and a_2 fixed, and b_1 and b_2 varied. (e, f): With the values of b_1 and b_2 fixed, and a_1 and a_2 varied

The part we analyze two populations, Group 1 and Group 2, represented by blue and red curves, respectively. The changes are plotted under three scenarios. (a, b): The seasonal factors differ. In the left graph, their values range from 0 to 0.5, while in the right graph, the values are increased to 0.5 to 1. We are observed that the final epidemic scale increases significantly with the increase of seasonal factors. (c, d): With a_1 and a_2 held constant, and b_1 and b_2 varied, we are found that the final epidemic scale F increases with the increase of b_1 and b_2 , with a generally average effect (e, f): With and held constant, and a_1 and a_2 varied, we are found that the final epidemic scale F increases with the increase of a_1 and a_2 , with a generally average effect. The parameters used are $\omega = 0.8, \phi_1 = \varepsilon = 0.9, \phi_2 = 0.5$.

For Group 1: $S_1 = 10^5, V_1 = 3 \times 10^4, I_1 = 8 \times 10^3, L_1 = 3 \times 10^3, N_1 = 10^6$.

For Group 2: $S_2 = 10^5, V_1 = 4 \times 10^4, I_1 = 9 \times 10^3, L_1 = 5 \times 10^3, N_1 = 10^6$.

From these three rows of graphs, we are evident that as the number of patients increases and seasonal factors rise, the scale of the flu outbreak significantly increases.

Finally, the relationship graph depicting the final scale of five different groups and the total population over time, as well as the relationship between the final epidemic scale and seasonal factors a_1, a_2, b_1, b_2 is simulated (see Figure 4 and see Figure 5), revealing a positive correlation between the final epidemic scale and seasonal factors.

4.3. Different years in China and seasonal factors impact

Here, we through that the influenza infection situations of different age groups from 2004 to 2019 are simulated based on public health scientific data. As can be seen from see Figure 6, see Figure 7, see Figure 8 and see Figure 9, during the period from 2004 to 2011, teenagers were the group most severely affected by the flu. In the following years, the infant population and the middle-aged population also followed closely behind. Looking at the graph in this section, we can see that the number of people suffering from the flu has been increasing year by year since 2012, reaching a peak in 2019 (see Figure 10). In 2020, it slowed down. We speculate that this might be related to the novel coronavirus that was prevalent in 2019, which led to a continuous decline in the immunity of the population and caused the number of people suffering from the flu to reach its maximum.

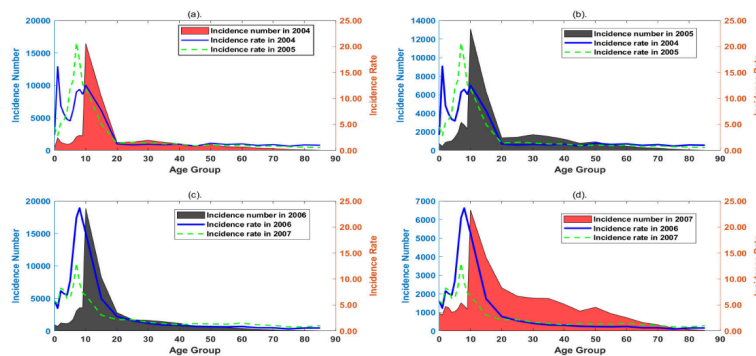


Figure 6. The number of cases and the incidence rate of influenza during 2004 - 2007 were plotted respectively with the area chart on the left vertical axis and the curve chart on the right vertical axis. Here, the horizontal axis represents different age groups. (a). Shows the number of cases of influenza in 2004 and the incidence rate in 2004 and 2005; (b). Shows the number of cases of influenza in 2005 and the incidence rate in 2004 and 2005; (c). Shows the number of cases of influenza in 2006 and the incidence rate in 2006 and 2007; (d). Shows the number of cases of influenza in 2007 and the incidence rate in 2006 and 2007. From the figure, it can be seen that teenagers aged 12 - 20 are more likely to be infected with the influenza virus

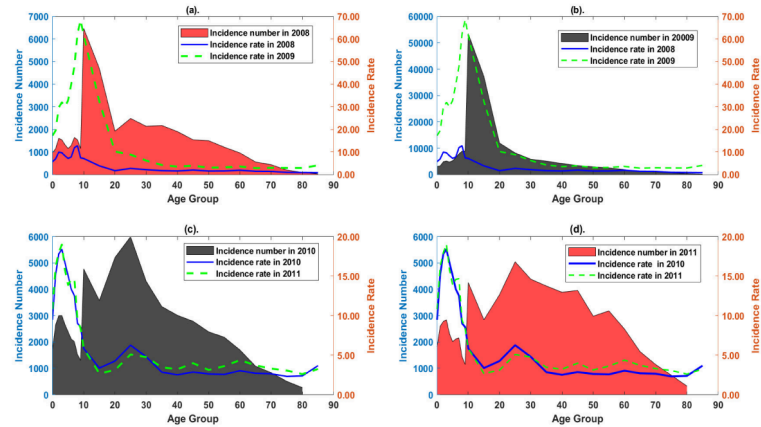


Figure 7. The number of cases and the incidence rate of influenza during 2008 - 2011 were plotted, respectively, using the area chart on the left vertical axis and the curve chart on the right vertical axis. Here, the horizontal axis represents different age groups. (a). Shows the number of cases of influenza in 2008 and the incidence rate in 2008 and 2009; (b). Shows the number of cases of influenza in 2009 and the incidence rate in 2008 and 2009; (c). Shows the number of cases of influenza in 2010 and the incidence rate in 2010 and 2011; (d). Shows the number of cases of influenza in 2011 and the incidence rate in 2010 and 2011. From the graph, it can be seen that teenagers aged 10 - 20 are more likely to be infected with the influenza virus

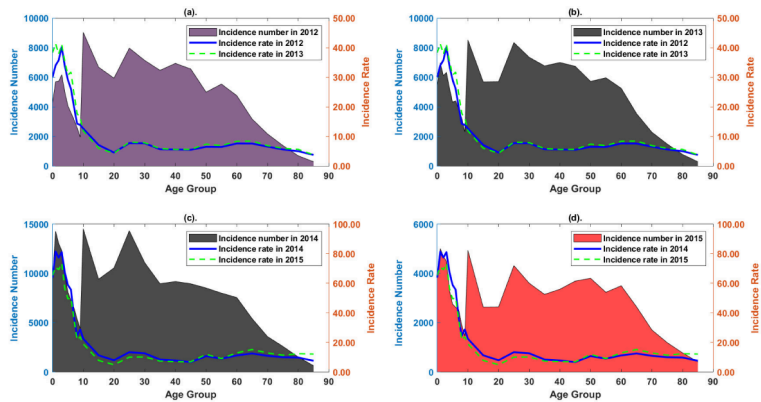


Figure 8. The number of cases and the incidence rate of influenza during 2012 - 2015 were plotted, respectively, using the area chart on the left vertical axis and the curve chart on the right vertical axis. Here, the horizontal axis represents different age groups. (a). Shows the number of cases of influenza in 2012 and the incidence rate in 2012 and 2013; (b). Shows the number of cases of influenza in 2013 and the incidence rate in 2012 and 2013; (c). Shows the number of cases of influenza in 2014 and the incidence rate in 2014 and 2015; (d). Shows the number of cases of influenza in 2015 and the incidence rate in 2014 and 2015. As can be seen from the chart, infants and toddlers aged 0-10, as well as young adults aged 12-50, young adults, middle-aged adults are more likely to be infected with the influenza virus

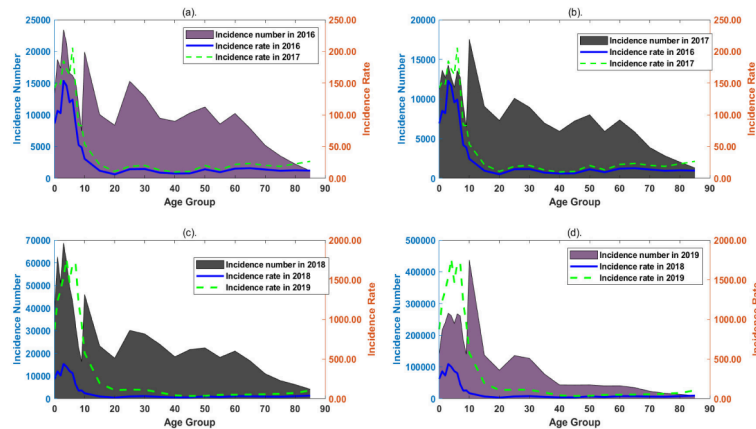


Figure 9. The number of cases and the incidence rate of influenza during 2016 - 2019 were plotted, respectively, using the area chart on the left vertical axis and the curve chart on the right vertical axis. Here, the horizontal axis represents different age groups. (a). Shows the number of cases of influenza in 2016 and the incidence rate in 2016 and 2017; (b). Shows the number of cases of influenza in 2017 and the incidence rate in 2016 and 2017; (c). Shows the number of cases of influenza in 2018 and the incidence rate in 2018 and 2019; (d). Shows the number of cases of influenza in 2019 and the incidence rate in 2018 and 2019. As can be seen from the chart, infants and toddlers aged 0-10, as well as young adults aged 12-60, young adults, middle-aged adults are more likely to be infected with the influenza virus

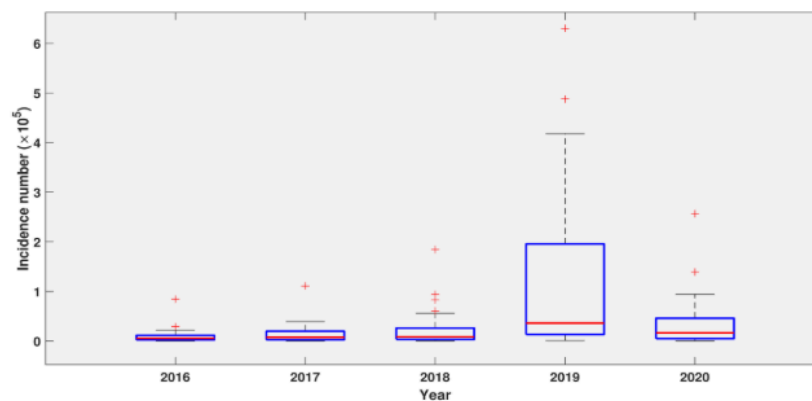


Figure 10. The number of people infected with influenza in China from 2016 to 2020 has been plotted. The vertical axis represents the number of infections and the horizontal axis represents different years. From the graph, it can be seen that 2019 was the year with the most severe influenza infection in China, followed by 2020 and 2018. Compared with 2016 and 2017, the number of infections was relatively smaller

In order to explore the relationship between the influenza cases in different years in China and seasonal factors, we further organize these data. By establishing the heritage algorithm and parameter fitting methods, combined with the model (3), we calculate the approximate values of the relevant seasonal factors for the influenza epidemic from 2004 to 2019 about every year different age groups. We will population division four different age groups incident: 1. Infancy and early childhood (0-15), 2. Adolescence (16-30), 3. Middle age (31-50), 4. Old age (51-85), as see Table 1 and see Table 2.

From the calculation results, it can be seen that the seasonal factor of the influenza virus showed an upward trend from 2004 to 2019. Combined with the numerical simulation results analyze in the previous two sections: the seasonal factor is positively correlated with the basic reproduction number of the influenza disease and the final epidemic scale for model (3). Here, we also verify the accuracy of this conclusion.

Table 1. Seasonal factors for influenza diseases among different age groups (2004-2011)

Year	Age Group	a1	a2	b1	b2
2004	1	0.44	1.24	0.39	$1 \cdot 10^{-2}$
2004	2	$1 \cdot 10^{-2}$	0.55	$1 \cdot 10^{-2}$	$1 \cdot 10^{-2}$
2004	3	6.75	8.36	1.91	4.44
2004	4	$1 \cdot 10^{-2}$	$1 \cdot 10^{-2}$	0.44	$1 \cdot 10^{-2}$
2005	1	$1 \cdot 10^{-2}$	0.1	1.15	0.5
2005	2	2.59	0.67	0.4	$1 \cdot 10^{-2}$
2005	3	$1 \cdot 10^{-2}$	$1 \cdot 10^{-2}$	0.28	$1 \cdot 10^{-2}$
2005	4	0.7	$1 \cdot 10^{-2}$	2.49	0.19
2006	1	$2.2 \cdot 10^{-2}$	$3.58 \cdot 10^{-2}$	$3.73 \cdot 10^{-2}$	9.99
2006	2	$1.12 \cdot 10^{-2}$	$1.16 \cdot 10^{-2}$	$1.01 \cdot 10^{-2}$	10
2006	3	$2.11 \cdot 10^{-2}$	$1.57 \cdot 10^{-2}$	$2.22 \cdot 10^{-2}$	$1.86 \cdot 10^{-2}$
2006	4	$1.02 \cdot 10^{-2}$	$1 \cdot 10^{-2}$	$1.42 \cdot 10^{-2}$	8.88
2007	1	$1 \cdot 10^{-2}$	$8.25 \cdot 10^{-2}$	$7.8 \cdot 10^{-2}$	9.99
2007	2	$1.32 \cdot 10^{-2}$	$3.03 \cdot 10^{-2}$	$2.12 \cdot 10^{-2}$	10
2007	3	$1 \cdot 10^{-2}$	$1 \cdot 10^{-2}$	$2.28 \cdot 10^{-2}$	$1.45 \cdot 10^{-2}$
2007	4	$1.45 \cdot 10^{-2}$	$1.72 \cdot 10^{-2}$	$1 \cdot 10^{-2}$	10
2008	1	$1.96 \cdot 10^{-2}$	$1.57 \cdot 10^{-2}$	$1.87 \cdot 10^{-2}$	10
2008	2	$1 \cdot 10^{-2}$	$4.27 \cdot 10^{-2}$	$6.18 \cdot 10^{-2}$	9.87
2008	3	$1 \cdot 10^{-2}$	$1 \cdot 10^{-2}$	$1.31 \cdot 10^{-2}$	$7.35 \cdot 10^{-2}$
2008	4	$1.56 \cdot 10^{-2}$	$2.66 \cdot 10^{-2}$	$1.33 \cdot 10^{-2}$	10
2009	1	$1 \cdot 10^{-2}$	1	0.81	$1 \cdot 10^{-2}$
2009	2	0.57	$1 \cdot 10^{-2}$	$1 \cdot 10^{-2}$	0.32
2009	3	2.03	1.48	$1 \cdot 10^{-2}$	0.66
2009	4	1.08	$1 \cdot 10^{-2}$	$1 \cdot 10^{-2}$	$1 \cdot 10^{-2}$
2010	1	$1 \cdot 10^{-2}$	$1 \cdot 10^{-2}$	$1 \cdot 10^{-2}$	$1 \cdot 10^{-2}$
2010	2	0.44	$1 \cdot 10^{-2}$	1.84	0.42
2010	3	1.01	1.2	$1 \cdot 10^{-2}$	$1 \cdot 10^{-2}$
2010	4	0.45	$1 \cdot 10^{-2}$	1.16	2.03
2011	1	4.66	1.19	5.21	0.55

Table 1. Continued

2011	2	7.29	7.83	7.28	0.91
2011	3	0.95	0.31	$1 \cdot 10^{-2}$	$1 \cdot 10^{-2}$
2011	4	0.9	$1 \cdot 10^{-2}$	$1 \cdot 10^{-2}$	$1 \cdot 10^{-2}$

Table 2. Seasonal factors for influenza diseases among different age groups (2012-2019)

Year	Age Group	a1	a2	b1	b2
2012	1	$1 \cdot 10^{-2}$	$1 \cdot 10^{-2}$	$1 \cdot 10^{-2}$	1.12
2012	2	0.97	$1 \cdot 10^{-2}$	$4.2 \cdot 10^{-2}$	$1 \cdot 10^{-2}$
2012	3	$9.29 \cdot 10^{-2}$	$1 \cdot 10^{-2}$	$1 \cdot 10^{-2}$	1.63
2012	4	$1 \cdot 10^{-2}$	$1 \cdot 10^{-2}$	0.52	$1 \cdot 10^{-2}$
2013	1	$6.76 \cdot 10^{-2}$	6.84	3.89	1.22
2013	2	3.82	1.96	2.19	4.63
2013	3	$1 \cdot 10^{-2}$	$1 \cdot 10^{-2}$	1.75	$1 \cdot 10^{-2}$
2013	4	8.33	2.8	6.72	3.95
2014	1	3.39	7.48	3.11	2.83
2014	2	$1 \cdot 10^{-2}$	$1 \cdot 10^{-2}$	$1 \cdot 10^{-2}$	2.57
2014	3	9.45	7.43	8.96	2.74
2014	4	0.55	$1 \cdot 10^{-2}$	0.43	$1 \cdot 10^{-2}$
2015	1	3.32	0.64	2.16	6.12
2015	2	0.34	$1 \cdot 10^{-2}$	$1 \cdot 10^{-2}$	2.56
2015	3	$1 \cdot 10^{-2}$	$1 \cdot 10^{-2}$	1.52	0.14
2015	4	$1 \cdot 10^{-2}$	$1 \cdot 10^{-2}$	0.61	0.43
2016	1	0.53	$1 \cdot 10^{-2}$	$1 \cdot 10^{-2}$	0.86
2016	2	0.12	0.72	$1 \cdot 10^{-2}$	$1 \cdot 10^{-2}$
2016	3	4.06	7.02	0.75	6.11
2016	4	$1 \cdot 10^{-2}$	$1 \cdot 10^{-2}$	0.55	$1 \cdot 10^{-2}$
2017	1	$1 \cdot 10^{-2}$	$1 \cdot 10^{-2}$	0.31	1.12
2017	2	$1 \cdot 10^{-2}$	$2.04 \cdot 10^{-2}$	$1 \cdot 10^{-2}$	$1 \cdot 10^{-2}$
2017	3	1.78	3.82	7.91	6.97
2017	4	$1 \cdot 10^{-2}$	$1 \cdot 10^{-2}$	0.48	$1 \cdot 10^{-2}$
2018	1	$1 \cdot 10^{-2}$	0.22	1.07	0.28
2018	2	9.47	6.83	4.61	8.18
2018	3	0.31	$1 \cdot 10^{-2}$	0.59	$1 \cdot 10^{-2}$
2018	4	1.06	6.58	6.62	0.55
2019	1	7.6	0.31	8.81	3.41
2019	2	7.58	6.51	4.96	4.24
2019	3	$1 \cdot 10^{-2}$	$1 \cdot 10^{-2}$	$1 \cdot 10^{-2}$	$1 \cdot 10^{-2}$
2019	4	0.58	$1 \cdot 10^{-2}$	0.36	$1 \cdot 10^{-2}$

4.4. Different provinces in China and seasonal factors impact

Here, we base the influenza infection situations in different regions from 2016 to 2020 are simulated based on public health scientific data. From see Figure 11 and see Figure 12, we simulate the prevalence of influenza diseases in different regions of China from 2016 to 2020. It can be seen that in different regions of China,

2019 was the year with the most severe influenza cases and also the year with the highest influenza incidence rate. At the same time, we also find that from 2016 to 2020, the provinces in China that have the highest number of flu disease cases are Guangdong, Zhejiang, Hunan, Beijing and Hubei in sequence; while the provinces with the highest incidence of flu diseases are Beijing, Zhejiang, Hunan and Shaanxi in sequence. To verify the relationship between the influenza infection situation in these provinces and seasonal factors, we also organize these data. By establishing the heritage algorithm and performing parameter fitting methods, combined with the model (3), We have evaluated the seasonal factors of the influenza model (3) for the top six regions in China from 2016 to 2020. They are as follows see Table 3, see Table 4, see Table 5, see Table 6, see Table 7.

Table 3. The top 5 provinces with the highest seasonal factors in 2016

Province	a1	b1	a2	b2
National	0.0043	0.0022	0.0121	0.0079
Hebei	0.0047	0.0088	0.0065	0.0094
Anhui	0.0047	0.0095	0.0058	0.0103
Shanxi	1.0420	1.0806	1.0000	1.0145
Jilin	1.1074	0.8278	0.1393	0.0518
Beijing	1.1105	1.0191	1.1021	1.0426

Table 4. The top 5 provinces with the highest seasonal factors in 2017

Province	a1	b1	a2	b2
National	2.2281	1.0000	201205	1.4276
Jiangsu	3.3281	1.0303	0.0078	0.0334
Gansu	1.0000	1.0553	1.0250	1.1017
iQinghai	1.0002	1.0021	1.0154	1.0015
Ningxia	1.0038	1.0110	1.0056	1.0000
Anhui	1.1105	11.0451	1.0174	1.0111

Table 5. Top 6 provinces by seasonal factors in 2018

Province	a1	b1	a2	b2
Zhejiang	1.1491	0.6757	0.9844	0.0166
National	1.2873	1.0363	1.1608	1.2237
Beijing	1.0000	1.0635	1.2643	1.4626
Inner Mongolia	0.1191	0.0215	0.0035	0.2429
Gansu	0.1122	0.0427	0.0742	0.0580
Ningxia	0.0156	0.0156	0.2526	0.3521

Table 6. Top 6 provinces by seasonal factors in 2019

Province	a1	b1	a2	b2
Tibet	5.7707	7.9847	2.1339	8.1892
Ningxia	5.8377	7.1719	3.6979	3.8630
Shaanxi	0.7244	6.5898	5.5467	6.7507
Hubei	7.3258	0.2478	9.3724	7.5720
Guizhou	6.8550	4.8189	6.2269	5.3843
Xinjiang	5.2425	6.2896	4.1100	5.8216

Table 7. Top 6 provinces by seasonal factors in 2020

Province	a1	b1	a2	b2
Ningxia	8.1365	1.1517	0.5032	8.6334
Gansu	8.3451	9.7689	7.2199	7.1330
Fujian	9.9124	6.9288	6.1445	1.1525
Hebei	9.9494	1.6681	3.3224	5.2511
Jiangsu	8.9256	7.4050	3.9326	6.2461
Guangxi	9.3779	7.5363	1.0476	9.9308

Where we fixed the remaining parameters in the model (3) as see Table 12. From the calculation results, it can also be seen that the seasonal factors are positively correlated with the basic reproduction number of the influenza disease and the final epidemic scale. In this section, we can verify this conclusion.

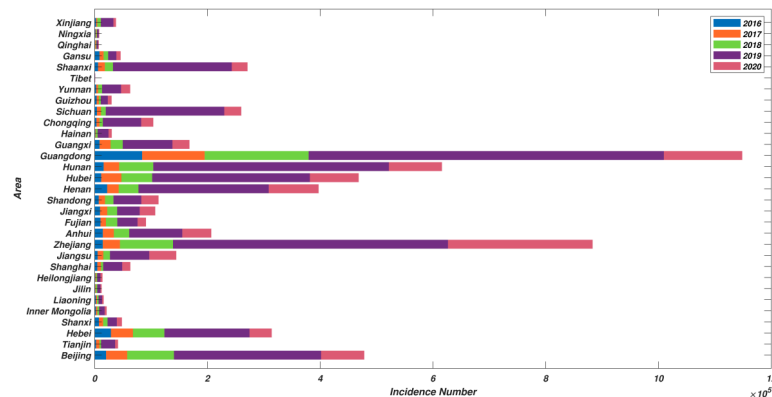


Figure 11. The chart illustrates the number of influenza infections in different provinces of China from 2016 to 2020. The vertical axis on the left represents different provinces of China, while the horizontal axis represents the incidence number. The colors of different bar charts represent different years. As can be seen from the chart, Guangdong Province is the region with the largest number of influenza infections in China, followed by Zhejiang Province, Hunan Province and Beijing Province, and Hubei Province

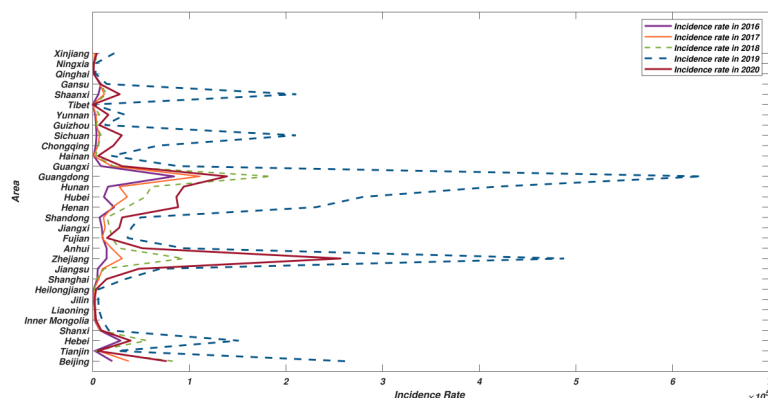


Figure 12. The incidence rates of influenza in different provinces of China from 2016 to 2020 have been plotted. The vertical axis on the left represents different provinces of China, while the horizontal axis represents the incidence rates. Different colored curves represent different years. From the figure, it can be seen that Beijing Province is the region with the highest incidence rate of influenza in China, followed by Zhejiang Province, Hunan Province and Shaanxi Province

Below is the result we obtained by using the data provided by the Public Health Science Data Center to calculate the corresponding seasonal factors of the SVEIRL model for influenza incidence in different provinces of China during the period from 2016 to 2020 (Tables 8-12).

Table 8. Seasonal factors for influenza virus in different Chinese provinces in 2016

Province	a1	b1	a2	b2
National	0.0043	0.0022	0.0121	0.0079
Beijing	1.1105	1.0191	1.1021	1.0426
Tianjin	1.6010	0.0107	0.0208	0.0177
Hebei	0.0047	0.0088	0.0065	0.0094
Shanxi	1.0420	1.0806	1.0000	1.0145
Inner Mongolia	0.0281	0.0407	0.0301	0.0274
Liaoning	0.0096	0.0099	0.0367	0.1004
Jilin	1.1074	0.8278	0.1393	0.0518
Heilongjiang	0.1827	0.0222	0.0478	0.0456
Shanghai	0.0053	0.0040	0.0018	0.0079
Jiangsu	1.0156	0.0236	0.0066	0.0278
Zhejiang	0.0069	0.0078	0.0042	0.0098
Anhui	0.0047	0.0095	0.0058	0.0103
Fujian	0.0154	0.0597	0.0170	0.2256
Jiangxi	1.0068	0.3951	0.5373	1.0236
Shandong	0.0229	0.0139	0.0684	0.0945
Henan	0.0039	0.0073	0.0625	0.1289
Hubei	0.0117	0.0110	0.0039	0.0303
Hunan	2.9216	0.0116	0.0144	0.8585
Guangdong	0.0030	0.0026	0.0000	0.0164
Guangxi	0.0176	0.0181	0.0560	1.0218

Table 8. Continued

Hainan	0.0333	0.5518	0.0076	0.0102
Chongqing	0.0027	0.0158	0.0139	0.0012
Sichuan	0.0133	0.0081	0.0058	0.0092
Guizhou	0.0086	0.0052	0.0138	0.0312
Yunnan	0.0087	0.0129	0.0090	0.0097
Tibet	0.0084	0.0091	0.0246	0.0039
Shaanxi	0.0039	0.0039	0.0039	0.0049
Gansu	0.0035	0.1308	0.2652	0.0595
Qinghai	0.0066	0.0146	0.0068	0.0261
Ningxia	0.0067	0.0078	0.2719	0.0975
Xinjiang	0.0041	0.0195	0.0010	0.3605

Table 9. Seasonal factors for influenza virus in different Chinese provinces in 2017

Province	a1	b1	a2	b2
National	2.2281	1.0000	2.1205	1.4276
Beijing	1.0000	1.0238	1.0496	1.0376
Tianjin	1.0807	1.0045	1.0586	1.2135
Hebei	1.0791	1.0000	1.5000	2.0458
Shanxi	0.0080	0.0096	0.0957	0.1041
Inner Mongolia	0.0431	0.0237	0.0123	0.0140
Liaoning	0.0095	0.0093	0.0078	0.0060
Jilin	0.0025	0.0066	0.0089	0.0143
Heilongjiang	1.1090	1.0053	1.0066	1.0083
Shanghai	0.0082	0.0040	0.0078	0.0045
Jiangsu	3.3281	0.0303	0.0078	0.0334
Zhejiang	0.0049	0.0072	0.0057	0.0046
Anhui	1.1007	1.0451	1.0174	1.0111
Fujian	0.0306	0.0068	0.1250	0.1004
Jiangxi	1.0113	1.0521	1.0027	1.0000
Shandong	0.0086	0.0099	0.0984	0.1066
Henan	0.0309	0.0126	0.0229	0.7085
Hubei	0.0081	0.0075	0.0025	0.0547
Hunan	1.0021	1.0309	1.0000	1.0460
Guangdong	0.0107	0.0039	0.0043	0.0074
Guangxi	0.0055	0.0082	0.0081	0.0088
Hainan	0.0040	0.0091	0.0065	0.0289
Chongqing	0.0011	0.0139	0.0096	0.0079
Sichuan	0.0071	0.0303	0.0055	0.0051
Guizhou	0.0145	0.0088	0.0097	0.0953
Yunnan	0.0079	0.0625	0.0078	0.1250
Tibet	0.0083	0.0576	0.0098	0.0607
Shaanxi	0.5496	0.0068	0.0095	0.0100
Gansu	1.0000	1.0553	1.0250	1.1017
Qinghai	1.0002	1.0021	1.0154	1.0015

Ningxia	1.0038	1.0110	1.0056	1.0000
Xinjiang	0.8873	0.0452	0.0472	0.2331

Table 10. Seasonal factors for influenza virus in different Chinese provinces in 2018

Province	a1	b1	a2	b2
National	1.2873	1.0363	1.1608	1.2237
Beijing	1.0000	1.0635	1.2643	1.4626
Tianjin	0.0078	0.0072	0.0071	0.0076
Hebei	0.0173	0.0253	0.0274	0.0136
Shanxi	0.0078	0.0069	0.0273	0.1016
Inner Mongolia	0.1191	0.0215	0.0035	0.2429
Liaoning	0.0098	0.0166	0.0111	0.1104
Jilin	0.0297	0.0360	0.0065	0.0284
Heilongjiang	0.0033	0.0096	0.0119	0.0091
Shanghai	0.0259	0.0244	0.0077	0.0938
Jiangsu	0.0126	0.0090	0.0098	0.0845
Zhejiang	1.1491	0.6757	0.9844	0.0166
Anhui	0.0087	0.0091	0.0063	0.0061
Fujian	0.0154	0.0451	0.7639	1.0050
Jiangxi	0.2069	0.0098	0.0098	0.0287
Shandong	0.0156	0.0151	0.0039	0.0088
Henan	1.0000	1.1430	1.2325	1.1875
Hubei	0.0113	0.0132	0.0007	0.0099
Hunan	1.1468	0.8113	1.1298	1.3162
Guangdong	0.0061	0.0061	0.0042	0.0057
Guangxi	0.0099	0.0098	0.0091	0.0037
Hainan	1.0262	1.0126	1.0105	1.0069
Chongqing	0.0053	0.0089	0.0083	0.0208
Sichuan	0.0122	0.0144	0.0562	0.0350
Guizhou	0.0089	0.0086	0.0099	0.0093
Yunnan	0.0078	0.0278	0.0978	0.1509
Tibet	0.0070	0.0141	0.0078	0.0047
Shaanxi	0.0113	0.0042	0.0089	0.0117
Gansu	0.1122	0.0427	0.0742	0.0580
Qinghai	0.0125	0.0105	0.0039	0.0160
Ningxia	0.0156	0.0156	0.2526	0.3521
Xinjiang	0.0096	0.0097	0.1036	0.0983

Table 11. Seasonal factors for influenza virus in different Chinese provinces in 2019

Province	a1	b1	a2	b2
National	5.9475	6.7253	2.2042	9.4414
Beijing	2.0233	0.6775	1.3457	6.1347
Hebei	4.7289	8.7030	0.2842	3.5412
Shanxi	7.6210	6.3485	2.1205	2.6112
Inner Mongolia	5.4401	6.2335	6.7464	6.5334
Liaoning	4.2544	1.8226	6.9757	3.7835
Jilin	5.4403	3.5399	5.2784	6.7424
Heilongjiang	3.2701	3.5211	8.5014	5.5711
Shanghai	5.3630	3.6309	6.6992	0.1365
Jiangsu	5.1342	0.2075	1.8959	5.4175
Zhejiang	1.1082	0.2127	3.8743	5.1492
Anhui	0.5950	0.5438	2.1127	6.7852
Fujian	2.8490	5.6413	5.6474	6.5945
Jiangxi	0.9721	2.9976	1.9192	4.4703
Shandong	2.9273	2.9210	5.7266	5.8211
Henan	1.7153	7.8130	5.3934	6.7703
Hubei	7.3258	0.2478	9.3724	7.5720
Hunan	6.3961	0.0046	0.3527	6.5348
Guangdong	0.7145	8.9113	6.1278	1.3897
Guangxi	5.7966	6.5241	5.7755	7.6684
Hainan	2.5762	6.2323	5.7276	6.0241
Chongqing	0.6241	2.8094	6.3165	1.5000
Sichuan	0.5282	2.7836	4.1100	7.0647
Guizhou	6.8550	4.8189	6.2269	5.3843
Yunnan	0.8838	0.0940	6.8172	6.5675
Tibet	5.7707	7.9847	2.1339	8.1892
Shaanxi	0.7244	6.5898	5.5467	6.7507
Gansu	4.3820	4.8209	8.8527	8.1504
Qinghai	4.1500	5.4829	5.3759	9.6448
Ningxia	5.8377	7.1719	3.6979	3.8630
Xinjiang	5.2425	6.2896	4.1100	5.8216

Table 12. Seasonal factors for influenza virus in different Chinese provinces in 2020

Province	a1	b1	a2	b2	Value of μ
National	2.4098	1.8649	2.8389	0.3869	0.001
Beijing	5.2824	5.7002	9.0971	8.3578	0.002
Tianjin	5.3572	1.7509	8.8417	4.9125	0.0015
Hebei	9.9494	1.6681	3.3224	5.2511	0.001
Shanxi	6.7116	4.8326	5.1131	6.6561	0.001
Inner Mongolia	5.9197	4.8643	4.7185	8.9092	0.0005
Liaoning	6.3117	1.4908	3.5704	0.7022	0.0005
Jilin	7.5815	5.0922	8.1204	7.5177	0.0002

Table 12. Continued

Heilongjiang	4.5781	8.6953	8.1088	0.2962	0.0003
Shanghai	6.3535	1.9104	1.1721	8.3065	0.001
Jiangsu	8.9256	7.4050	3.9326	6.2461	0.0005
Zhejiang	0.7018	7.0519	8.8063	0.4944	0.0008
Anhui	7.6865	4.1053	2.5133	5.6464	0.0004
Fujian	9.9124	6.9288	6.1445	1.1525	0.0003
Jiangxi	3.7716	0.3922	1.5979	8.4833	0.0005
Shandong	8.7841	0.6537	1.6545	4.3032	0.0008
Henan	7.5932	1.8170	5.5232	5.1823	0.0006
Hubei	4.2655	4.6934	3.0418	4.8361	0.0007
Hunan	1.8174	3.4274	5.4760	4.5105	0.0009
Guangdong	5.5109	2.9190	5.2347	5.2789	0.001
Guangxi	9.3779	7.5363	1.0476	9.9308	0.0006
Hainan	3.7960	4.2936	2.5564	5.9273	0.0004
Chongqing	6.2281	3.5526	4.8657	1.9465	0.0005
Sichuan	1.5908	4.7304	8.0494	1.3738	0.0004
Guizhou	4.0232	1.8920	8.3501	1.2651	0.0003
Yunnan	5.1581	7.2424	7.0129	5.7704	0.0002
Tibet	7.0857	5.2823	8.1223	3.5479	0.0001
Shaanxi	4.5711	5.3913	6.8963	6.0858	0.0006
Gansu	8.3451	9.7689	7.2199	7.1330	0.0007
Qinghai	4.6767	2.1462	3.6996	0.0894	0.0005
Ningxia	8.1365	1.1517	0.5032	8.6334	0.0003
Xinjiang	2.4091	3.6229	5.3473	7.6741	0.0004

4.5. Flu scenarios kinds in China and seasonal factors impact

Here, we base on the data from the China Influenza Center, the types of influenza infections in south, north and nationwide in China from 2022 to 2024 are simulated (see Figure 13, see Figure 14, see Figure 15). We show 2022-2024 Relationship Diagram of Influenza Cases of Different Types in the North and South and Nationwide as a Percentage of Total Positive Cases. From the chart, we can be seen that in 2022, the number of flu infections in southern China is higher than in northern China. The majority of flu infections in the south occur in June. At the same time, the number of people infect with type A influenza throughout the year accounted for a larger proportion of the total positive cases compared to those infected with type B influenza. In 2023, the number of flu infections in northern China is higher than in southern China. The majority of flu infections in the north occur in March. At the same time, the number of people infect with type A influenza throughout the year accounted for a larger proportion of the total positive cases compared to those infected with type B influenza. In 2024, the number of flu infections in southern China is higher than in northern China. The majority of flu infections in the south occur in December, while in the north and nationwide, the majority of flu infections occur in January. At the same time, the number of people infect with type A influenza throughout the year accounted for a larger proportion of the total positive cases compared to those infected with type B influenza. Specifically, the A(H3N2) subtype has the highest proportion, followed by the A(H1N1) pdm09 subtype, and then the Victoria lineage of type B, with the B/Yamagata lineage not being differentiated. By establishing nonlinear least squares fitting method, combined with the model (3), we also calculate the approximate values of the seasonal factors related to the Flu scenarios kinds in China: the

A(H3N2) subtype, the A(H1N1) pdm09 subtype, the B subtype. They are as follows see Table 13, see Table 14, see Table 15.

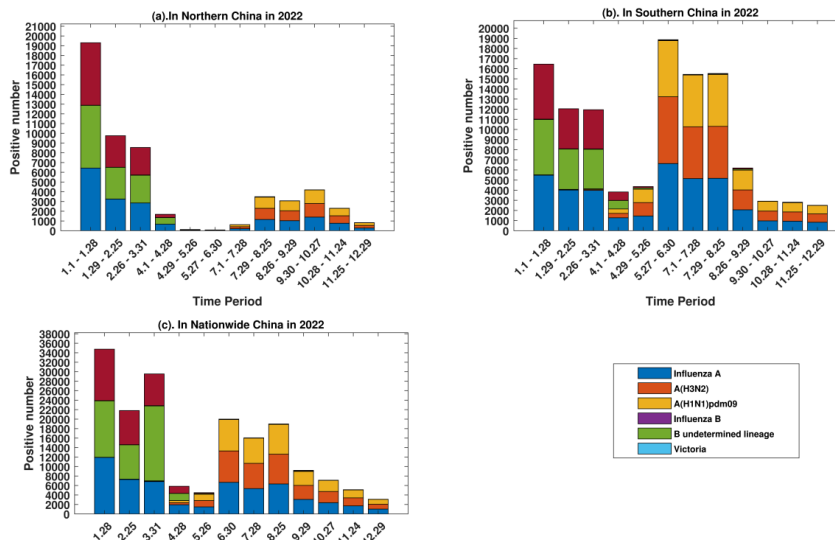


Figure 13. 2022 Relationship Diagram of Influenza Cases of Different Types in the North and South and in China as a Percentage of Total Positive Cases: This chart illustrates the monthly distribution of influenza cases of different type in the northern (a) and southern regions (b) of China, as well as nationwide (c), as a percentage of total positive cases throughout the year 2022. Various types of flu cases are denoted by bars of different colors

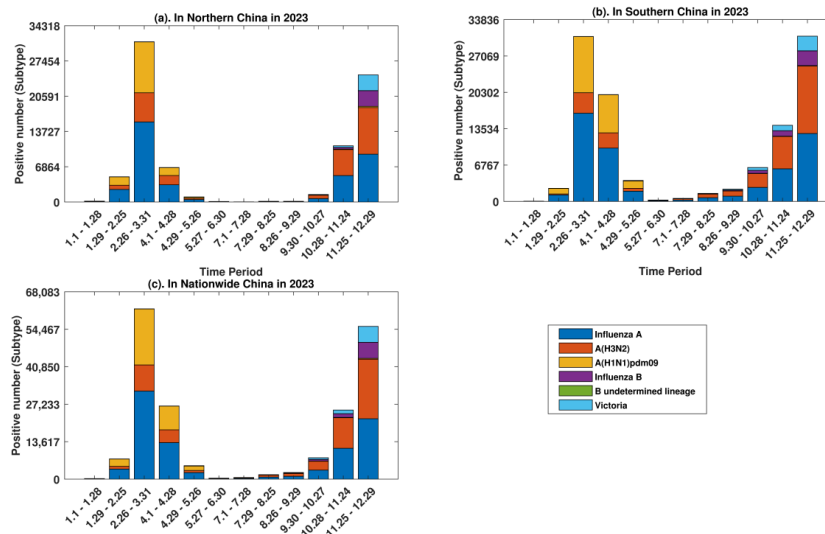


Figure 14. 2023 Relationship Diagram of Influenza Cases of Different Types in the North and South and in China as a percentage of Total Positive Cases: This chart illustrates the monthly distribution of influenza cases of different types in the northern (a) and southern regions (b) of China, as well as nationwide (c), as a percentage of total positive cases throughout the year 2023. Various types of flu cases are denoted by bars of different colors

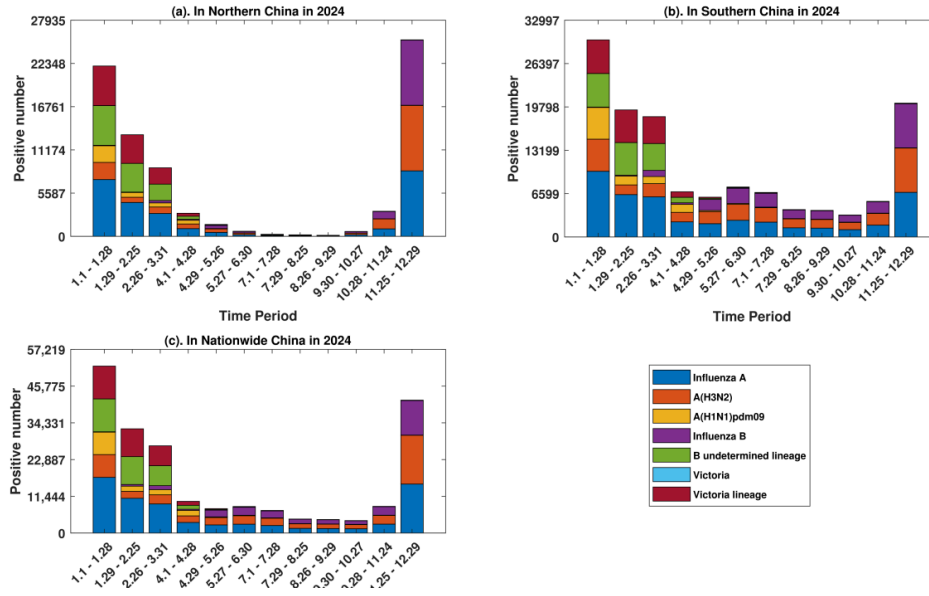


Figure 15. 2024 Relationship Diagram of Influenza Cases of Different Types in the North and South and in China as a Percentage of Total Positive Cases: This chart illustrates the monthly distribution of influenza cases of different types in the northern (a) and southern regions (b) of China, as well as nationwide (c), as a percentage of total positive cases throughout the year 2024. Various types of flu cases are denoted by bars of different colors

Table 13. Seasonal factors for different influenza types in 2024

Influenza Type	a1	b1	a2	b2
Positive	0.5	0.5	0.5	0.5
A type	0.5	0.5	0.5	0.5
A_H3N2	0.5	0.5	0.5	0.5
A_H1N1_pdm09	0.5	0.5	0.5	0.5
B type	0.5	0.5	0.5	0.5
B subtype	0.5	0.5	0.5	0.5
Victoria	0.5	0.5	0.5	0.5

Table 14. Seasonal factors for different influenza types in 2023

Influenza Type	a1	b1	a2	b2
Victoria	0.5	0.51623	0.5149	0.5
B subtype	0.5	0.51599	0.51518	0.5
B type	0.5	0.51622	0.51489	0.5
A_H1N1_pdm09	0.5	0.51024	0.50945	0.5
A_H3N2	0.5	0.51683	0.51355	0.5
A type	0.5	0.5164	0.51333	0.5
Positive	0.5	0.51568	0.51159	0.5

Table 15. Seasonal factors for different influenza types in 2022

Influenza Type	a1	b1	a2	b2
Victoria	0.5	0.51973	0.51841	0.5192
B subtype	0.5	0.53142	0.53089	0.53202
B type	0.5	0.51673	0.5142	0.51498
A H1N1 pdm09	0.5	0.53144	0.53093	0.53205
A H3N2	0.5	0.53153	0.53283	0.53407
A type	0.5	0.53154	0.53283	0.53407
Positive	0.5	0.52825	0.52816	0.52942

Table 16. Seasonal factors for ILI (%) North and South in 2022-2025

Year	Region	a1	b1	a2	b2
2022-2023	South	3.5031	0.82819	0.54744	0.49834
2022-2023	North	3.5857	0.83202	0.55012	0.49916
2023-2024	South	5.253	1.5116	0.56984	0.51321
2023-2024	North	5.4437	1.5364	0.57642	0.51457
2024-2025	South	4.9376	1.314	0.57218	0.51297
2024-2025	North	5.0871	1.336	0.57615	0.51349

We divide a year into 52 weeks. The data shows that the seasonal factors of different types of influenza fluctuated around 0.5 from 2022 to 2024. Among them, the seasonal factor in 2022 was the largest. From the calculation results, it can also be seen that the seasonal factors are positively correlated with flu influenza disease. In this section, we can also verify this conclusion.

4.6. ILI (%) of south and north in China and seasonal factors impact

Here, we base on the data from the China Influenza Center, the ILI (%) situations in the southern and northern regions from 2022 to 2025 are simulated (see Figure 16). We take the year is divided into 52 weeks, with each week serving as the time unit. From the chart, we can be seen that from 2022 to 2023 and from 2023 to 2024, the ILI (%) ratio of influenza infections in southern China is higher than that in northern China. In 2024 to 2025, the ILI (%) ratio of influenza infections in northern China is higher than that in the south.

Meanwhile, the ILI (%) for influenza in both northern and southern China is highest throughout the year 2023 to 2024. From a yearly perspective, influenza in both northern and southern China mainly occurs during weeks 10 to 20 and 45 to 52, which corresponds to late February to early June and late October to early December, with a concentration in the spring and winter seasons. By establishing nonlinear optimization methods and least square methods, combined with the model (3), we also calculate the approximate values of the seasonal factors related to ILI (%) of south and north in China about different years. They are as follows see Table 16. Similarly, we divide the year into 52 weeks. The data shows that the seasonal factor was the highest in the period from 2023 to 2024. From the calculation results, we can also verify this conclusion: The seasonal factors are positively correlated with flu influenza disease.

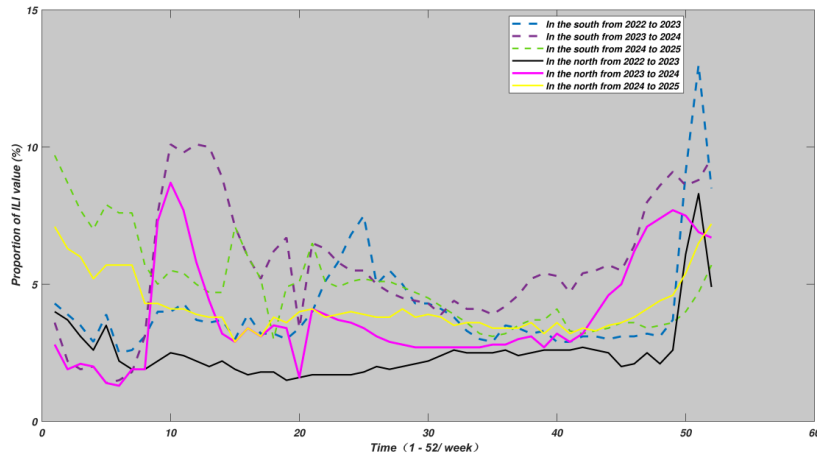


Figure 16. The ratio of ILI (%) for influenza in the north and south from 2022 to 2025. This chart, based on influenza data provided by sentinel hospitals in China, depicts the ILI (%) ratio of influenza in northern and southern China from 2022 to 2025. The dash line represents the northern region, while the solid line represents the southern region. The year is divided into 52 weeks, with each week serving as the time unit

5. Conclusion

This study examines the global public health burden of seasonal influenza, emphasizing that it is caused by the influenza virus, characterized by acute respiratory infections, distinct seasonality, and significant annual morbidity and mortality. Furthermore, numerical simulations indicate a significant positive correlation between seasonal factors and the basic reproduction number, and the final epidemic size.

The study proposes a mathematical model to estimate the seasonal Influenza focuses on the SVEIRL model with seasonal fluctuations, considering seasonal driving factors with a period of T , including baseline contact rates a_1, a_2 , and seasonal forcing magnitude b_1, b_2 . And the essay discusses the dynamical behavior of the SVEIRL model for seasonal infectious, including positivity and boundedness, disease-free equilibrium points P_0 , reproduction number R_0 and the final epidemic size F , the calculations indicate a positive correlation between the seasonal factors and both the basic reproduction number and the final epidemic size.

Finally, to further verify the relationship between them, through numerical simulations are conducted by adjusting the relevant parameters, and it is found that as seasonal factors increase, the basic reproduction number R_0 and the final epidemic scale F will correspondingly increase. When the number of susceptible individuals is much greater than the number of infected individuals, the disease will continue to outbreak for a period of time. When the number of infected individuals is almost the same as the number of infected individuals, the disease will outbreak on a small scale for a period of time and then stabilize in the region. When the number of infections is less than the number of cases, the disease will eventually disappear over time.

At the end of the article, based on data from the China Influenza Center and the Public Health Science, the study conducts simulations on the influenza situation in China and incorporates the data into the SVEIRL model. Then estimate the ranges of seasonal factors for influenza in China under different scenarios, including different years in China and seasonal factors impact, different provinces in China and seasonal factors impact, Flu scenarios kinds in China and seasonal factors impact and ILI (%) of South and north in China and seasonal factors impact. By establishing the heritage algorithm and parameter fitting methods, nonlinear optimization

and least square methods, combined with the SVEIRL model, the study calculate the approximate values of the seasonal factors related to the influenza epidemic in Chinese these different scenarios and once again confirm that there is a positive correlation between the seasonal factors and the scale of the influenza epidemic.

The seasonal influenza model proposed in this paper requires extensive experimental validation to confirm its effectiveness. Future research could incorporate more experiments to test the accuracy of the model. Currently, the focus is primarily on seasonal influenza in China, but future studies could include case analyses from more regions to explore effective strategies to deal with seasonal influenza in different areas.

References

- [1] Tamerius, J., Nelson, M. I., Zhou, S. Z., Viboud, C., Miller, M. A., & Alonso, W. J. (2011). Global influenza seasonality: Reconciling patterns across temperate and tropical regions. *Environmental Health Perspectives*, *119*, 439–445.
- [2] Fu, X., He, H., Chen, Z., Cha, Y., & Yun, L. (2014). Analysis of the role of different age groups in influenza epidemics. *Chinese Journal of Public Health*, *30*, 1466–1469.
- [3] El Hajji, M., Alshaikh, D. M., & Almualllem, N. A. (2023). Periodic behaviour of an epidemic in a seasonal environment with vaccination. *Mathematics*, *11*, 2350.
- [4] Coletti, P., Poletto, C., Turbelin, C., Blanchon, T., & Colizza, V. (2018). Shifting patterns of seasonal influenza epidemics. *Scientific Reports*, *8*(1), 12786.
- [5] Xie, Y., Lin, S., Zeng, X., Tang, J., Cheng, Y., Huang, W., Li, J., & Wang, D. (2003). Two peaks of seasonal influenza epidemics — China. *CCDC Weekly*, *36*.
- [6] Barnea, O., Yaari, R., Katriel, G., & Stone, L. (2011). Modelling seasonal influenza in Israel. *Mathematical Biosciences*, *8*, 561–573.
- [7] Wenger, J. B., & Naumova, E. N. (2010). Seasonal synchronization of influenza in the United States older adult population. *PLOS ONE*, *5*(11), e10187.
- [8] World Health Organization. (2009). *Influenza research agenda for public health* (1st ed.). Author.
- [9] World Health Organization. (2006). *WHO rapid advice guidelines on pharmacological management of humans infected with avian influenza A (H5N1) virus*. Author.
- [10] China Center for Disease Control and Prevention. (n.d.). *China influenza surveillance weekly report*. Retrieved from official website of China CDC.
- [11] Stegehuis, C., van der Hofstad, R., & van Leeuwen, J. S. H. (2016). Epidemic spreading on complex networks with community structures. *Nature Communications*, *6*, 29748.
- [12] Zhang, Q., & Wang, S. (2020). Analysis of influenza epidemic characteristics among different age groups in the eastern Beijing area during winter and spring seasons from 2016 to 2019. *Journal of Laboratory Medicine and Clinical Medicine*, *9*, 17.
- [13] Gabrick, E. C., Brugnago, E. L., de Souza, S. L. T., Iarosz, K. C., & Batista, A. M. (2024). Impact of periodic vaccination in SEIRS seasonal model. *Journal of Theoretical Biology*, *174*(3).
- [14] Shaman, J., & Karspeck, A. (2012). Forecasting seasonal outbreaks of influenza. *Proceedings of the National Academy of Sciences*, *109*(50), 20425–20430.
- [15] Nsoesie, E. O., Beckman, R. J., Shashaani, S., Nagaraj, K. S., & Marathe, M. V. (2013). A simulation optimization approach to epidemic forecasting. *PLOS ONE*, *8*(6), e67164.
- [16] Stollenwerk, N., Spaziani, S., Mar, J., Eguiguren, I., Knopof, D., & Cusimano, N. (2022). Seasonally forced SIR systems applied to respiratory infectious diseases, bifurcations, and chaos. *Scientific Reports*, *12*, 3556043.
- [17] Wagner, J., Bauer, S., Contreras, S., Fleddermann, L., Parlitz, U., & Priesemann, V. (2023). Societal feedback induces complex and chaotic dynamics in endemic infectious diseases. *arXiv*.

- [18] Tildesley, M. J., & Keeling, M. J. (2009). Is R_0 a good predictor of final epidemic size: Foot-and-mouth disease in the UK. *Journal of Theoretical Biology*, 82–4.
- [19] Bacaër, N., & Gomes, M. G. M. (2009). On the final size of epidemics with seasonality. *Bulletin of Mathematical Biology*, 71, 1954–1966.
- [20] Hinder, J., Assaf, M., & Schwartz, I. B. (2022). Outbreak size distribution in stochastic epidemic models. *Physical Review Letters*, 128(7), 078301.
- [21] Brauer, F. (1984). An introduction to networks in epidemic modeling. Department of Mathematics.
- [22] Fan, C., Liu, L., Guo, W., Yang, A., Ye, C., Repu Jilili, M., Ren, M., Xu, P., Long, H., & Wan, Y. (2020). Prediction of epidemic spread of the 2019 novel coronavirus driven by spring festival transportation in China: A population-based study. *Public Health*, 17(5), 1679.